

# EVOLUTION OF A SUITE OF SMART MILLIMETRE WAVE RADAR SYSTEMS FOR SITUATIONAL AWARENESS AND AUTOMATION IN MINES

Graham Brooker, Mark Bishop, Ross Hennessy

Australian Centre for Field Robotics

University of Sydney

Sydney Australia

Emails: gbrooker@acfr.usyd.edu.au, m.bishop@acfr.usyd.edu.au,  
r.hennessy@acfr.usyd.edu.au

*Abstract-This paper defines the issues required for the development of successful visualisation sensors for use in open cut and underground mines. It examines the mine environment and considers both the reflectivity of the rock and attenuation effects of dust and water droplets. Millimetre wave technology, as an alternative to the more commonly used laser and sonar implementations, is selected due to its superior penetration through adverse atmospheric conditions. Of the available radar techniques, frequency modulated continuous wave (FMCW) is selected as being the most robust. The theoretical performance of a number of 94GHz FMCW millimetre wave radar systems is determined and these confirm the capability of these sensors in the mining environment. The paper describes implementations of FMCW radar sensors for simple ranging, two dimensional line scanning and three dimensional imaging that are based on a common ranging module and in the case of the 2D and 3D applications, a common swash-plate mirror scanner. Data obtained during field trials in mines is presented to justify the selection of this technology*

**Index terms:** Millimetre wave radar, mining, range measurement, scanning, imaging, FMCW

## I. INTRODUCTION

This paper documents the evolution of a suite of millimetre wave radar sensors designed and developed to perform various measurement functions in a mining environment. These sensors must be capable of performing flawlessly 24 hours a day, 7 days a week irrespective of the conditions and optical visibility.

Development of reliable equipment to operate in an underground environment poses some unique design challenges. The air temperature in deep hard-rock mines can exceed 35°C which, coupled to a relative humidity close to 100% and mineral-rich dusts, results in a corrosive atmosphere. In conjunction with this, underground blasting produces strong concussions that travel through the mine. In open cut mines, the issues are slightly different

with most radars mounted on booms of large rope-shovels and draglines, where the harsh outdoor environment, percussive and vibrational effects are dominant.

### **The Applications**

Underground applications include the measurement of range in ore-passes and imaging of the internal structures of large mined out cavities called stopes that are often filled with dust or water vapour. In open cut mines, the uses of radar extend from 3D surface mapping for volume reconciliation and slope stability monitoring to bucket fill and bucket position measurement functions. High resolution millimetre wave radars are also poised to become the sensors of choice for situational awareness for haul trucks and other moving vehicles as mines become more automated.

Most underground mines operate by moving rock from the higher levels, where the mining takes place, through near vertical tunnels called ore-passes or silos to crusher stations at the lowest levels. This is illustrated schematically in Figure 1a. Loads of rock are dumped into the pass through a coarse lattice called a grizzly that restricts the maximum size to less than one metre across. In some mines this is via an inclined finger pass that feeds into the side of the main pass as illustrated in Figure 1a, whereas, in others, the grizzly covers the top of the main pass. Pass diameters vary between 3 and 6m while silo and stope diameters can be up to ten times this size.

The accurate measurement of the range to the ore in a pass allows for some automation of the ore flow process and to allow for the operator to maintain a rock buffer above the loading station, to monitor the volume of ore stored and primarily to check for “hung” passes. This last event occurs when the rock plugs the pass leaving an ever widening void as rock is drawn from below. If this condition is not detected in good time, thousands of tonnes of rock can fall onto the loading station, when the plug releases, with potentially catastrophic consequences.

Many underground mines, where bulk bodies of ore are found, produce large underground voids called stopes. Geotechnical constraints generally limit their size in plan to about 40×40m but not vertically where the limitation is the ore body outline, which might be up to 300m in extent. The void created by this mining operation must be filled with a competent material capable of standing while the stope adjacent to it is mined. The materials of choice are CAF (a weak concrete) and/or rock-fill, depending on the duty required. Because of the cost difference between filling with CAF and with rock, it would be lucrative if the amount of rock-fill could be maximised without compromising the strength of the stope.

The ideal tool for viewing the filling process is a “real-time” remote device that can see through the mist and vapour to monitor the levels of fill as shown in Figure 1b.

In surface mining applications, the primary function of draglines is to remove the overburden and uncover the coal, which can be removed by another dragline, shovel-truck system or front-end loader, for transport to crushers. This process is further complicated by the requirement that these massive machines, some weighing in excess of 3,500 tonnes, retain access to and from the working area.

The environments around draglines and rope shovels are often dusty or, in some cases, shrouded in mist, smoke or even steam, to the extent that the operator is unable to see the working area. This makes digging impossible for significant periods of time, which is extremely expensive for a machine that costs up to \$500,000 per day to operate. Once again, the ideal tool for viewing the dig and fill process is a “real-time” remote device that can see through the opaque environment to present the operator with an image of the terrain surface or the bucket contents as illustrated in Figure 1c and d. These visual feedback sensors can also be used for the partial and, ultimately, for the complete automation of the mining process.

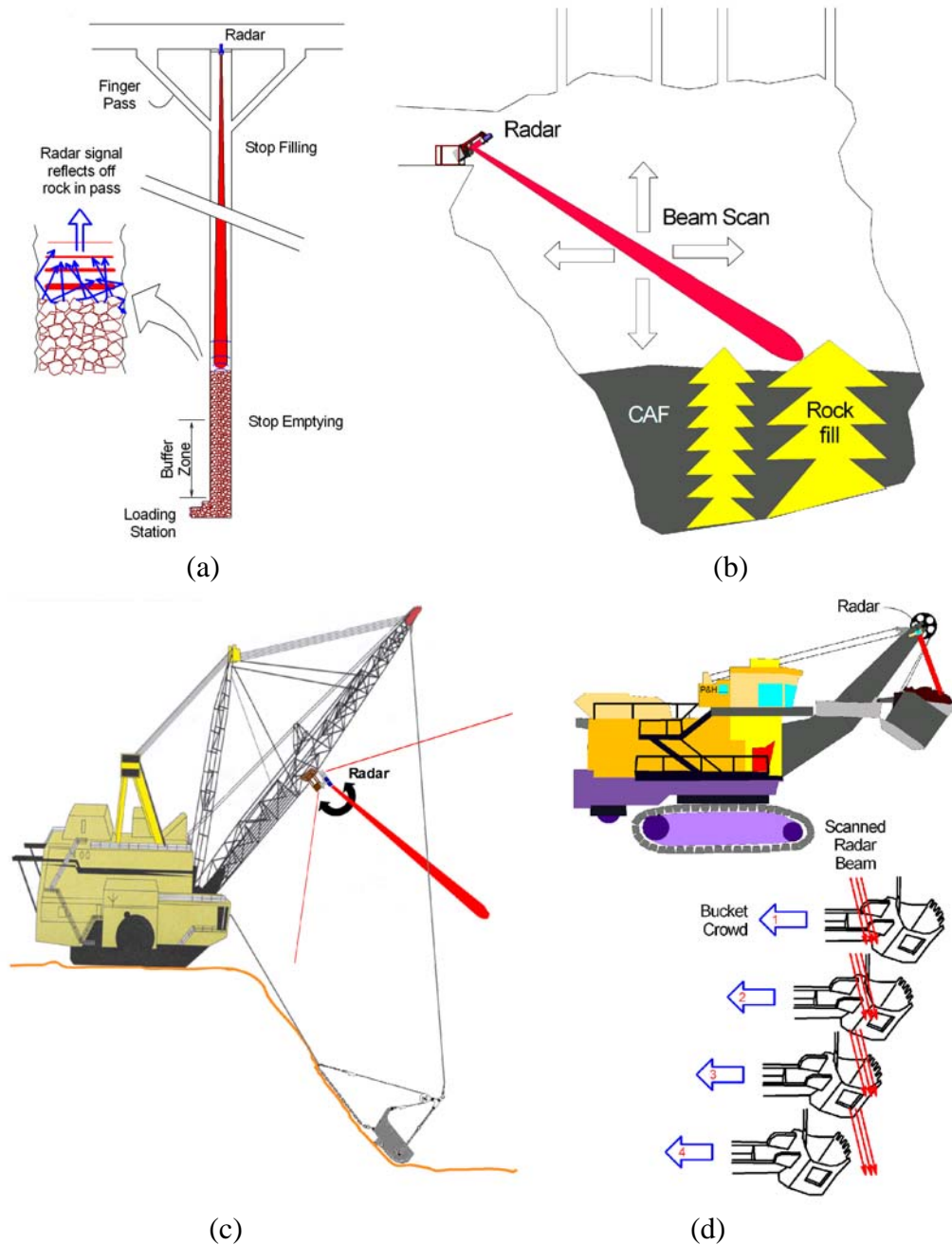


**Figure 1: Measurement applications for (a) Ore-pass showing the rock fill (b) Stope showing the CAF (concrete) and crushed rock fill, (c) Dragline monitoring of the dig area and the bucket position and (d) Rope shovel monitoring of the bucket fill and tooth integrity**

## II. SENSOR REQUIREMENTS

### Signal Dynamic Range

All four sensors shown in Figure 1 must be capable of measuring the range to the rock or backfill through an extremely dusty volume to an accuracy of better than 1% of the maximum range. Some stopes and passes are longer than 300m and the requirements for open-cut visualisation easily exceed this, so for a minimum range requirement of 3m (or less), a range ratio capability of at least 100 to 1 is required.

The relative received power can then be determined by application of the radar range equation,

$$S_{dB} = P_{dB} + 2G_{dB} + 10\log_{10}\left(\frac{\lambda^2}{(4\pi)^3}\right) + \sigma_{dB} - L_{dB} - 40\log_{10} R, \quad (1)$$

where:  $S_{dB}$  – Received power (dBW),  
 $P_{dB}$  – Transmitted power (dBW),  
 $G_{dB}$  – Antenna Gain (dB),  
 $\lambda$  – Carrier wavelength (m),  
 $\sigma_{dB}$  – Target radar cross section (dBm<sup>2</sup>),  
 $L_{dB}$  – Losses (dB),  
 $R$  – Range (m).

Most of these parameters are determined by the radar system design, however, the target radar cross section,  $\sigma_{dB}$ , is a function of the terrain reflectivity,  $\sigma^o$ , and the beam footprint.

It is possible to estimate the reflectivity of a typical distributed target (rock surface) using rough surface scattering models (Beckmann and Spizzichino 1987). Alternatively the following well known relationship (Nelson 2001) can be used to determine the relationship between the material permittivity (complex dielectric constant) for an homogenous sample and the reflectivity  $\sigma^o$

$$\sigma^o = \left| \frac{\cos \theta - \sqrt{\epsilon_{rock} - \sin^2 \theta}}{\cos \theta + \sqrt{\epsilon_{rock} - \sin^2 \theta}} \right|, \quad (2)$$

where  $\theta$  is the angle of incidence and the complex permittivity of the rock is  $\epsilon_{rock}$ .

Though not strictly valid for smooth surfaces, for a rough surface, where the average incidence angle  $\theta = 0^\circ$  the approximate reflectivity can be determined for coal at X-Band where  $\epsilon_{rock} = 4.21 - j0.156$  (Nelson 2001)

$$\sigma^o = \left| \frac{1 - \sqrt{\epsilon_{rock}}}{1 + \sqrt{\epsilon_{rock}}} \right| = 0.34, \quad (3)$$

As no measurements of permittivity could be found at frequencies higher than 10GHz, it must be assumed that this value is valid up into the millimetre wave band.

It has been found from measurement that the target structure and not the rock permittivity is dominant in determining the “effective” reflectivity and that it can vary from a couple of huge boulders or piles of blasted rock to liquid CAF. The measure shown in (3) is, therefore, not accurate in isolation and the radar cross-section,  $\sigma_{dB}$ , is usually determined experimentally. Figure 2 shows the results of more than 200 measurements made at 94GHz over a 24 hour period into a working pass being filled with dry rock with a reasonably constant permittivity. Variations of 30 to 40dB in target reflectivity can be seen (Brooker, Scheduling et al. 2005).

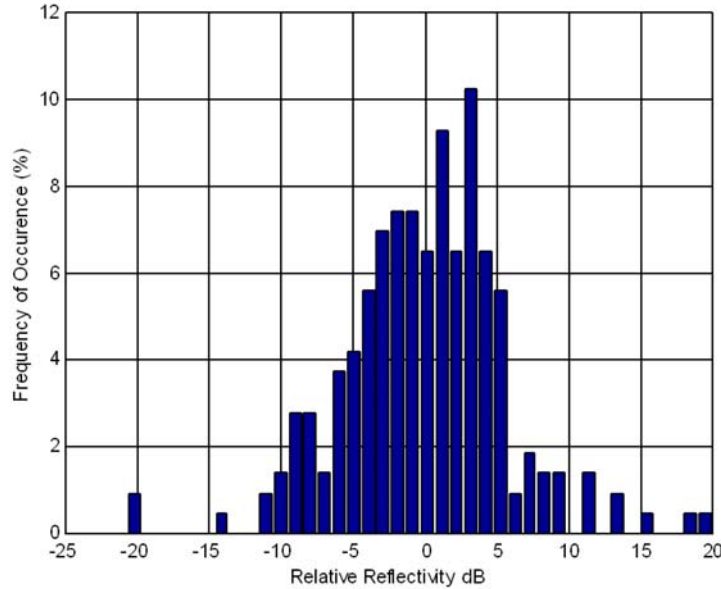


**Figure 2: Measured 94GHz reflectivity histogram made in a vertical ore-pass showing the large dynamic range in signal level that can be expected.**

As the radar cross section is the product of the target reflectivity and the area of the beam footprint,  $A_{foot}$ , for a symmetrical antenna with a half power beamwidth,  $\theta$ , at range,  $R$ , it is

$$\sigma_{dB} = 10\log_{10}(\sigma^o A_{foot}) = 10\log_{10} \sigma^o \frac{\pi}{4} (R\theta)^2 = \sigma_{dB}^o + 10\log_{10}\left(\frac{\pi\theta^2}{4}\right) + 20\log_{10} R. \quad (4)$$

Substituting into (1) results in

$$S_{dB} = P_{tdB} + 2G_{dB} + 10\log_{10}\left(\frac{\lambda^2}{(4\pi)^3} \cdot \frac{\pi\theta^2}{4}\right) - L_{dB} + \sigma_{dB}^o - 20\log_{10} R. \quad (5)$$

It is clear from (5) that a combination of 40dB of variation in the reflectivity, and a range ratio of 100 to 1 (40dB) results in a signal dynamic range of 80dB. To process this received power, the signal is generally digitised and hence an analog to digital converter (ADC) with a dynamic range of at least 80dB is required. As most common ADCs with the required throughput are 12bit devices, with a dynamic range of less than 72dB some form of gain control prior to conversion is required.

### Attenuation through Clouds of Dust and Water Droplets

Atmospheric attenuation through clear air is determined by frequency dependent molecular interactions with the electromagnetic radiation. In Figure 3, (Preissner 1978) it can be seen that the attenuation increases with increasing frequency in the microwave and millimetre wave bands before dropping off sharply into the IR and visible bands. In the millimetre wave band, windows of relatively low attenuation occur at 35 and 94GHz between oxygen absorption lines. It is within these windows that most radar activity occurs, with the frequency around 77GHz earmarked for automotive sensors and that around 94GHz reserved for military and experimental applications.

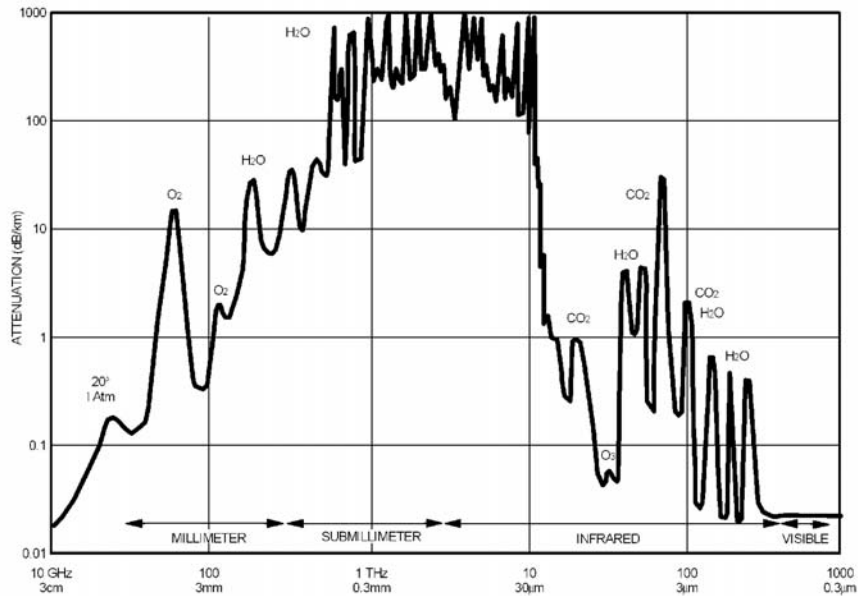


**Figure 3: Atmospheric attenuation of electromagnetic radiation in clear air as a function of frequency**

For the relatively short range applications considered in this paper, atmospheric attenuation is not significant. However, the effects of particulates suspended in the atmosphere are, and these are considered in the following section.

An interesting characteristic of almost all measured dust clouds is that the distribution of particle sizes is bimodal, as illustrated in Figure 4. This is apparently independent of the source of the dust, as it has been measured for wind blown dust (Patterson 1977; Pinnick, Fernandez et al. 1985), vehicle generated dust and dust generated by explosions (Pinnick, Fernandez et al. 1983). Unexpectedly, the distribution holds irrespective of the density of the dust cloud, though the proportions may change. Typical mass mean radii for the two peaks are between 1μm and 10μm for the fine dust and between 10μm and 50μm for the larger particles depending on the source of the dust.

The distribution of particle sizes hardly affects the attenuation in the microwave and millimetre wave bands because the wavelength is much larger than even the largest dust particle, so scattering can be accurately determined using the Rayleigh model. However, in the infrared and visible bands, the relative particle sizes are close to the wavelength and Mie scattering must be applied to model the attenuation.

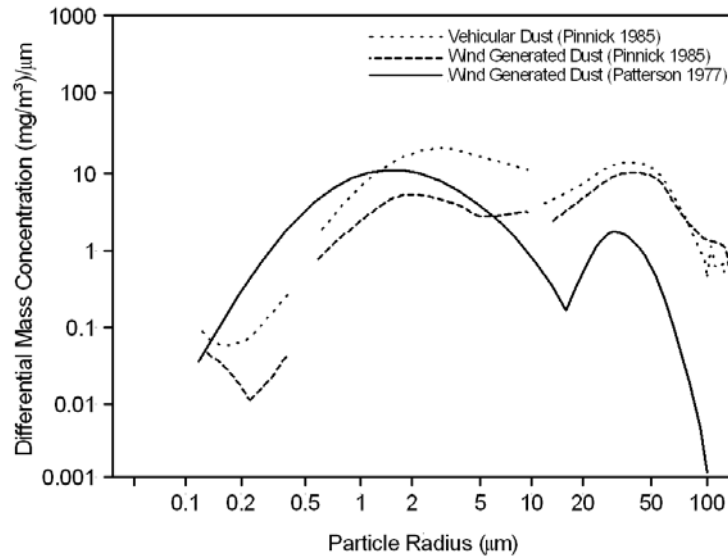


**Figure 4: Measured size distribution for vehicle generated and wind blown dust (Pinnick et al. 1985)**

As with water vapour, the density of dust and other particulates is often characterised according to the visibility of targets within that environment. Using this definition, it has been found that in wind-blown dust the visibility can be related to the mass of dust per cubic meter of air (mass loading) (Gillett 1979)

$$M_d = 37.3.V^{-1.07}, \quad (6)$$

where  $M_d$  is the mass loading of dust in  $\text{g/m}^3$  and  $V$  is the visibility in metres. The coefficients are dependent on the particle type and the meteorological conditions, and these have been selected as being typical for sand storms in the desert (Ghobrial and Sharief 1987).

**Table 1: Relationship between visibility and mass loading**

Visibility (m)	Mass Loading ( $\text{g/m}^3$ )
1	37
2**	17.8
5	8.5
50	0.57
100	0.27
1000	23 $\text{mg/m}^3$

\*\* Minimum visibility for heavy sand storm in Khartoum (Goldhirsh 2001)

According to(Pinnick et al. 1985), dust is mostly made up of clumps of finer particles so the individual density is lower than that of the actual rock material and seldom exceeds  $1.5\text{g/cm}^3$ . The density of the actual rock material varies from about  $2.75\text{g/cm}^3$  for limestone (Nelson 2001) down to  $2.44\text{g/cm}^3$  for quartz dust particles collected around Khartoum (Ghobrial et al. 1987) and  $1.8\text{g/cm}^3$  for sand with a 8% water content (Pinnick et al. 1985). The characteristics of coal are of importance in some industrial measurement applications, and it has a density of  $1.48\text{g/cm}^3$  (Nelson 2001).

Two mechanisms determine the attenuation of radar signals. They are  $\alpha_a$  (dB/km), the

attenuation due to absorption, and  $\alpha_s$  (dB/km), the attenuation due to scattering (Currie, Hayes et al. 1992)

$$\alpha_a = 81.86 \times 10^{-3} \frac{\text{Im}(-K)M_d}{\lambda\rho}, \quad (7)$$

$$\alpha_s = 1.353 \times 10^{-19} \frac{M_d a^3 K^2}{\lambda^4 \rho}, \quad (8)$$

where  $M_d$  (g/m<sup>3</sup>) is the mass loading,  $\rho$  (g/cm<sup>3</sup>) is the effective particle density,  $a$  ( $\mu$ m) is the particle radius and  $\lambda$  (m) is the wavelength.

$K$  is a constant determined by the dielectric properties of the material,

$$|K|^2 = \left| \frac{m^2 - 1}{m^2 + 2} \right|^2 = \left| \frac{\epsilon_r - 1}{\epsilon_r + 2} \right|^2, \quad (9)$$

where  $m$  is the complex index of refraction of the material.

In most cases the attenuation due to scattering is so small that it can be ignored, and the attenuation due to absorption can be determined in terms of the real component,  $\epsilon'$  and the imaginary component,  $\epsilon''$ , of the permittivity. These are also known respectively as the dielectric constant and the loss factor because the imaginary part is related to the rate at which energy is absorbed by the material.

For a material density of 2.44g/cm<sup>3</sup> and using the relationship between the mass loading and the visibility from equation (6), the attenuation can be rewritten in terms of the visibility (Ghobrial et al. 1987; Goldhirsh 2001),

$$\alpha_a = \frac{3.76\epsilon''}{\left[ (\epsilon' + 2)^2 + \epsilon''^2 \right] \lambda} V^{-1.07}. \quad (10)$$

Substituting into equation (10) for the permittivity of rock dust which has been measured to be  $\epsilon_{dust} = 5.23 - j0.26$  (Ghobrial et al. 1987) produces the result shown in Figure 5 at a wavelength of  $3.2 \times 10^{-3}$  m (94GHz). If the dust is replaced by water with a density of 1g/cm<sup>3</sup> and a permittivity  $\epsilon_w = 8.35 - j15.45$  (measured at 89GHz), the losses are much higher, as shown.

What is obvious from these results is that the total attenuation is extremely sensitive to the water content of the dust particles. As it is uncommon to find completely dry dust, significant variations in the attenuation can be expected in any measurements.

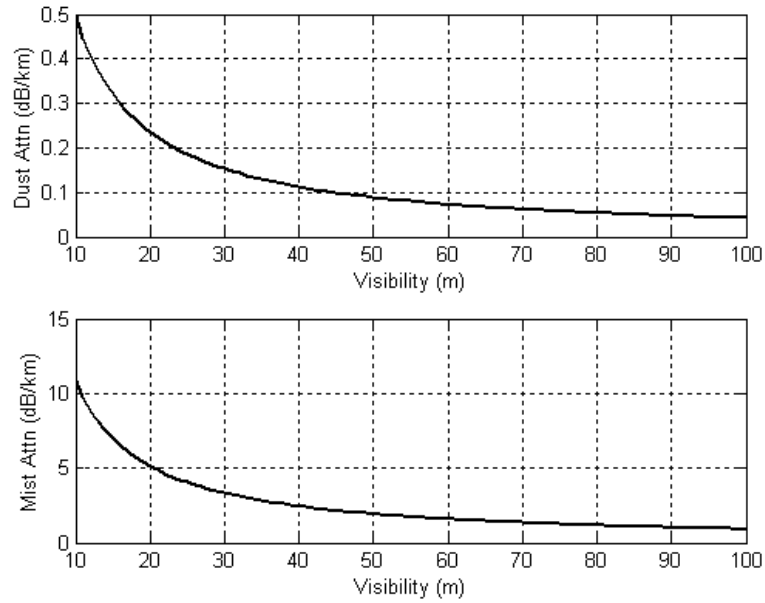


**Figure 5: Relationship between visibility and attenuation for dust and for mist droplets at 94GHz**

It can be seen that in contrast to the poor transmission at visible and IR wavelengths, at a wavelength of 3.2mm (94GHz), attenuations are practically negligible for short range operation through the dust. The losses do become significant in a water vapour environment if the visibility is very poor. For a visibility of 4m (extremely thick fog) which corresponds to a mass loading of 8.5g/m<sup>3</sup>, an attenuation of about 12dB/km can be expected.

To get a feel for the attenuation characteristics of lidar as compared to radar, the Table 2 (Brooker 2008) has been included.

**Table 2: Calculated attenuation through different aerosol types**

Source	Material	Density (g/cm <sup>3</sup> )	Mass conc (g/m <sup>3</sup> )	Visibility (m)	Attenuation (dB/km)	
					λ=3mm	λ=1-10μm
Desert Dust	Quartz	2.6	10	3.4	1.56	1300
Stack: Stone Mill	Quartz	2.6	80	0.5	12.5	10400
Stack: Steel Mill	Coal	1.5	10	3.4	2.2	1300
Volcanic Dust	Quartz	2.6	5	6.5	0.8	650
Light Fog	Water	1	0.001	7km	0.004	0.2
Heavy Fog	Water	1	1	55	4	200

**Backscatter from Clouds of Dust and Water Vapour**

The effectiveness of a laser or radar system is dependent not only on the actual signal level returned from the target of interest, but also the relative level of this signal in comparison to other competing returns at the same range. These competing signals are generally referred to as clutter.

The most common sources of clutter are returns from the dust or water droplets within the radar beam, or from large (high reflectivity) returns that enter through the sidelobes of the antenna. Analysis, which will not be repeated here, shows that backscatter from dust is of the order of 10<sup>-7</sup> (m<sup>2</sup>/m<sup>3</sup>) in the case of millimetre wave radar which is insignificant.

## **Other Considerations**

### Pass Blockages

In some applications there are partial blockages in the pass, and there are always falling rocks and/or falling water in both passes and cavities, all of which introduce spurious targets that must be discriminated against.

### Installation and Interfaces

Because the sensors are often mounted in inaccessible and dangerous areas, they should be light, easy to install both mechanically and electrically, easy to align and should require the minimum configuration setup. They should still remain as versatile as possible to cater for a wide variety of underground and surface configurations.

### Reliability and Safety

For the reasons outlined above, the sensors should be extremely reliable (MTBF >1 year of continuous operation), they should require no maintenance and their long term accuracy must be good. This is a tall order given the environmental extremes encountered, the blast concussion, machine vibration and the likelihood of rock falls. As regards safety, any radiation produced should be well within specified safety margins at the operational frequency.

### Manufacturing and Maintenance Issues

A wide variety of manufacturing issues must be considered during the development of these sensors. Components should be multi source. The electrical design should be robust enough to allow for component tolerances of 20% to provide for module replacement without recalibration.

Assembly should be simple and quick, with module as well as the complete unit quick to test and calibrate.

The design process should attempt to address all of the environmental issues including high ambient temperature, shock, vibration and dramatic changes in pressure as a result of the blast concussion. Issues of dust and water ingress as well as potential rock falls should be considered during the design of the housing.

As regards maintenance and repair, the primary issues that must be considered relate to fast, accurate fault diagnosis and system modularity, which allows the use of line replaceable units. These should be easy and quick to repair.

## **III. SELECTION OF THE TECHNOLOGY**

For many years, laser, acoustic and microwave radar systems have been the workhorse technologies for industrial level measurement and imaging. However, since the availability of moderately low-cost K and millimetre wave band components, these higher frequency options have become more popular (Brooker 1993; Kielb and Pulkrabek 1999). The pros and cons of each are summarised below:

### Laser

- Good in enclosed regions due to the narrow beam
- Robust, well established technology

- Low cost
- Poor penetration of dust and water vapour
- Poor sensitivity to low reflectivity materials
- Dust on antenna (lens) causes problems
- Small aperture and hence easy to scan using mirrors

#### Acoustic

- Low cost
- Poor in dust
- Can not meet range requirements
- Beam too wide for enclosed region
- Problems with extraneous noise
- Air currents affect propagation
- Problems with dust build-up on transducer
- Cannot be scanned using mirrors

#### Microwave radar

- Low cost
- Good penetration of dust and water vapour
- Dust on antenna not generally a problem
- Beam too wide for enclosed region in passes
- Beam too wide for accurate imaging in stopes
- Cannot easily be scanned using mirrors

#### Millimetre wave radar

- Good penetration of dust and water vapour
- Narrow beam good for enclosed areas
- Dust on antenna not generally a problem
- Sufficiently small aperture to scan using mirrors
- High cost

It has been shown (Brooker et al. 2005) that reliable and repeatable measurements can only be made in an ore-pass if the beam is sufficiently narrow that it does not illuminate the walls even at the longest operational range. Some commercial X-band (wide beam) radar systems have attempted to overcome this problem by storing lists of all the spurious returns that have been encountered in the empty pass or silo. This is effective if the range and amplitude of the spurious targets does not change. However in the ore-pass application, every time a load of rock is dumped into the pass, the walls are scoured, with the result that a new spurious table is required.

It is possible to be reasonably objective in determining the most cost-effective candidate technology for a particular application. For example, Figure 6 shows the criteria determined for an ore-pass radar. This is based on attenuations derived using the results presented in this paper and data from numerous studies on electromagnetic (Bhartia and Bahl 1984; Comparetto 1993; Perry and Baden 2000; Goldhirsh 2001) and acoustic (Goodsit 1982; Kue 1984) propagation through dust.

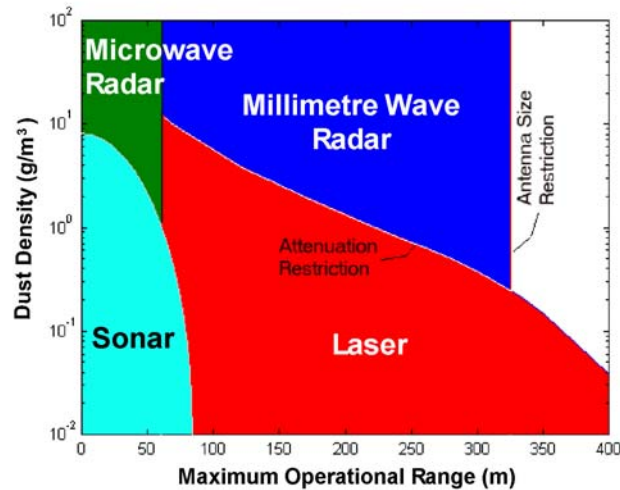


**Figure 4: Cost effective sensor selection for the Ore-pass radar operation for different ranges and dust densities**

For the ore-pass or stope-fill application where dust levels of about  $8\text{g/m}^3$  are commonplace, all four technologies are suitable if the range is short. However, for an operational range in excess of about 60m (common in underground mines), sonic systems do not achieve the required range unless clusters of transducers are used (Longbottom and Eren 1994), and the antennas for microwave radars become prohibitively large.

It should be noted that Figure 6 does not consider the effect of backscatter which, in laser systems, can result in the detection of spurious targets caused by reflections from higher than average dust concentrations. However such problems can be overcome to a large extent, by last-pulse processing which leaves attenuation as the major limitation to laser performance.

To produce accurate measurements in a cavity requires an extremely narrow beam. This is only available from either a large aperture or for high frequency operation. As large aperture devices are generally cumbersome and heavy, the only alternative is to use the highest possible frequency. Ultimately, millimetre wave radar is the only viable candidate for these applications.

For dragline and shovel based imaging systems, both millimetre wave and microwave frequencies can be used. However, the smaller aperture requirements, and hence lower overall size and weight, make the millimetre wave option the more practical, albeit more expensive. In many above ground installations, the size requirement is not an issue and a number of quite large microwave and millimetre wave systems have been constructed for imaging and slope stability applications (Reeves, Sticklely et al. 2000; Macfarlane and Robertson 2004).

A number of different millimetre wave radar techniques have been applied to measure range in industrial processes as described in the following section.

### **Narrow Pulse**

Many implementations of pulsed radar technology for industrial measurement applications have been developed (WeiB and Knochel 1997; Motzer 2000). In general, these systems are designed to measure liquid levels at short range and thus do not offer the sensitivity nor sufficient range for most mining applications.

A real pulse with a duration  $\tau = 10\text{ns}$  is required to obtain a resolution of about 1.5m. Because it is difficult to produce high peak powers using solid state amplifiers and because a pulse

time-bandwidth product  $B \cdot \tau \approx 1$  is required for matched filtering of the received echo (Barton 1976), the operational range of such systems is limited.

For example, for a reasonable cost solid state transmitter operating at 94GHz, the peak power is limited to 5W from a single IMPATT diode operating at a PRF of 500 kHz. This translates into an average power of only 25mW.

A radar based on this technology was built (see Figure 7) and installed over a 300m long, narrow, ore-pass for evaluation.

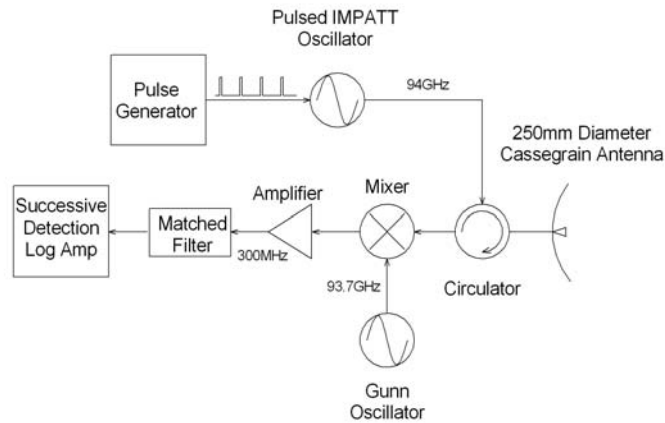


**Figure 7: Pulsed millimetre wave radar configuration**

Its performance was good as shown in the measured profile in Figure 8. However the IMPATT oscillator maintenance requirements were too high because of concussion induced component drift. Recent advances in IMPATT diode and packaging technology have made this technology more practical for use in inhospitable environments and applications may well appear in the future.

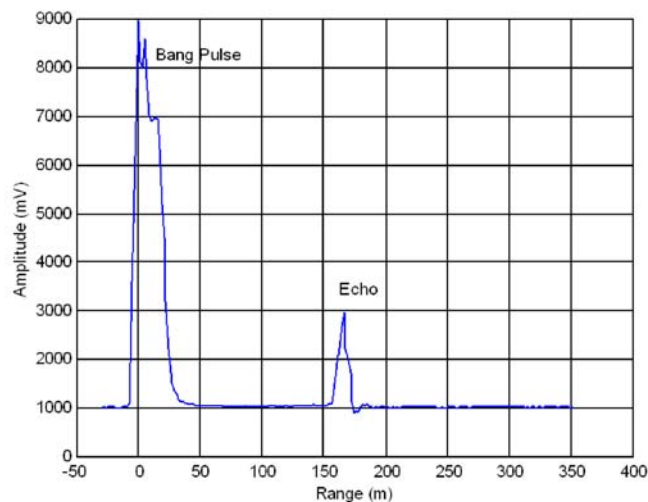


**Figure 8: Ore-pass Echo Profile Obtained using a Pulsed W-Band Radar**

Alternative methods of obtaining high resolution with a short blanking range include FM and stepped frequency techniques (Currie and Brown 1987). In essence, they increase the time-bandwidth product to improve the resolution while still offering good range performance.

### Stepped Frequency

A technique that avoids many of the high speed data acquisition problems of narrow pulse radars is the pulse-to-pulse stepped frequency mode. An appropriate pulse width,  $\tau$ , is selected, for example a 100ns pulse will span a range of 15m. The frequency of each pulse is then shifted by an amount  $\Delta F$  from that of the previous pulse, where  $\Delta F$  is about  $1/2\tau = 5\text{MHz}$  to ensure that there is no phase ambiguity from pulse to pulse in the return.

After each pulse is transmitted, the received echo in a particular 15m range-gate is coherently detected, and the amplitude and phase information stored. For transmit frequency,  $F_1$ , the phase of the received echo is

$$\Phi_1 = \frac{4\pi F_1 R}{c}. \quad (11)$$

For a static target, the phase of the next pulse echo transmitted at a frequency of  $F_2$  will be  $\Phi_2$ . For a sequence of pulses equally spaced in frequency, there is a predictable pulse to pulse phase shift of  $\delta\Phi$  that is a function of the frequency difference  $\Delta F = F_2 - F_1$ .

$$\delta\Phi = \frac{4\pi R \Delta F}{c} \quad (12)$$

This pulse-to-pulse phase shift appears as an apparent Doppler frequency, which can be analysed using the FFT (Currie et al. 1987) or the MUSIC algorithm (Li, Li et al. 1998) to obtain the improved resolution.

The total unambiguous range after processing is  $c/2\Delta F$  and the range resolution is  $c/2F_{tot}$  where  $F_{tot}$  is the total frequency excursion of the transmitted signal. For a sequence of  $N$  pulses,  $F_{tot} = N\Delta F$ . For an ultimate resolution of 1.5m,  $F_{tot} = 100\text{MHz}$ ,  $\Delta F = 5\text{MHz}$  and  $N = 20$  samples.

The average power increases to 250mW due to the longer transmit time at the same PRF if a peak power of 5W is again transmitted and in addition the sampling and digitisation requirements are improved by a factor of ten from 10ns to 100ns. However, the blanking range is increased to at least 15m to avoid overlapping the transmit and receive cycles.

### Frequency Modulated Continuous Wave

Frequency Modulated Continuous Wave (FMCW) radars have been used for many years in the industrial process control arena. However, as with pulsed radar technology, most systems have been developed for short range measurement of liquid levels in tanks (Brumbi 1995; Blied and Pulkrabek 1999). This technology has been adapted for longer range low-cost industrial applications by increasing the operational frequency to the 24GHz ISM band (Zimmermann and Wiesbeck 1996), as well as for automotive applications at a range of frequencies including the now standard 76-77GHz band (Groll and Detlefsen 1997).

As illustrated in Figure 9, most FMCW radars operate by transmitting a linear frequency chirp,  $\Delta f$ , of long duration,  $T_b$ . At any time, the received echo is shifted in frequency from the transmitted signal by the product of the roundtrip time to the target,  $T_p$ , and the rate of change of frequency,  $S = \delta f / \delta t$ . If the received signal is mixed with a portion of the transmitted signal and filtered, the resulting output will be a constant beat frequency  $f_b$ .

Two factors limit the range resolution of these systems: the first is a function of the chirp bandwidth,  $\Delta f$ , and the second is the actual linearity that is achieved for the transmitted chirp.

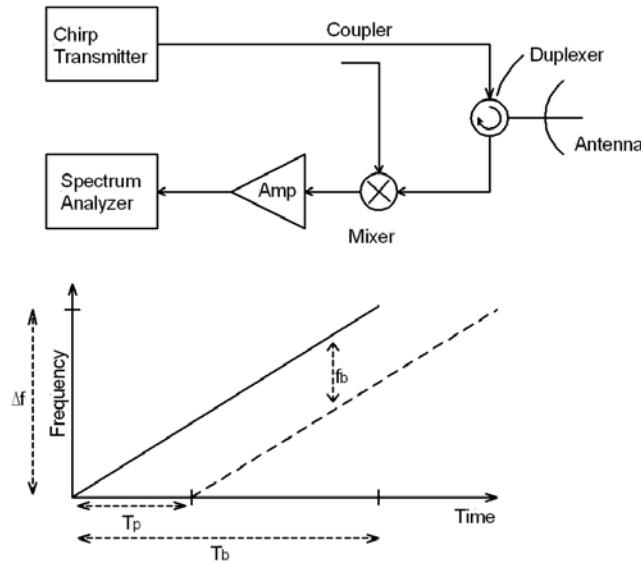


**Figure 9: FMCW radar schematic diagram and operational principles**

A moderate-resolution radar system may have a chirp bandwidth,  $\Delta f = 100\text{MHz}$ , and a sweep time of 2ms. The range resolution that can be achieved, if only the chirp bandwidth considered, is

$$\delta R_{chirp} = \frac{c}{2\Delta f} = \frac{3 \times 10^8}{2 \times 100 \times 10^6} = 1.5\text{m} . \quad (13)$$

For a rate of change of frequency,  $S$  (z/s), at any point on the graph, the linearity,  $Lin$ , is defined as

$$Lin = \frac{S_{max} - S_{min}}{S_{min}} . \quad (14)$$

The resolution that can be achieved is the product of the linearity and the range to the target if the chirp nonlinearity is quadratic in nature (Brooker 2005). Thus for a target range of 150m and a linearity of 0.01 (1%), the resolution would also be 1.5m.

The two results can be combined in quadrature to determine the ultimate system range resolution

$$\delta R = \sqrt{\delta R_{chirp}^2 + \delta R_{lin}^2} = 2.12\text{m} . \quad (15)$$

The beat frequency for a radar with these characteristics at a range of 300m is the product of the round trip time to the target and the chirp slope

$$f_b = T_p \frac{\partial f}{\partial t} \approx T_p \frac{\Delta f}{T_b} = \frac{2R}{c} \frac{\Delta f}{T_b} = 100\text{kHz} , \quad (16)$$

making the relationship between the measured beat frequency and the range

$$\frac{R}{f_b} = \frac{T_b c}{2\Delta f} = 0.003\text{m/Hz} . \quad (17)$$

Since a number of targets can be present in the beam at one time, spectrum analysis is used to extract all of the frequencies generated in the received signal. This function is usually

implemented in software using the FFT process, though some research has been conducted into the effectiveness of other techniques (Liau, Carr et al. 1986; Pichler, Gulden et al. 2003).

If the signal is observed for a time  $T_b = 2\text{ms}$  then the width of a frequency bin  $W = 1/T_b = 500\text{Hz}$  (1.5m) and the main lobe width, shown in Figure 10, is twice that. The 3dB bandwidth of the filter produced by this process is 0.89 bins (1.33m) for no windowing, increasing to 1.3 bins (1.95m) for a Hamming window (Kirsten 1979).

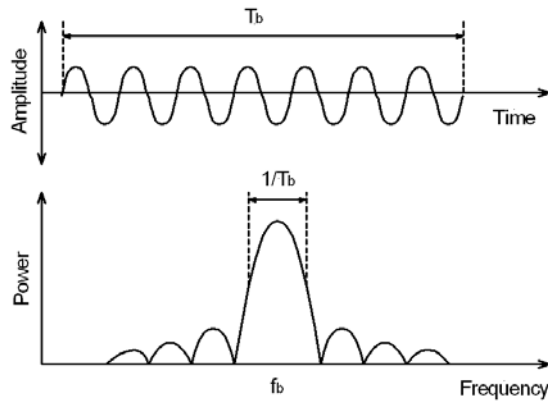


**Figure 10: Relationship between the observation time and the width of the received target spectrum**

Because the FMCW radar transmits continuously, the average and peak powers are the same and these are limited to about 25mW due to signal leakage effects (Ondria and Cardiasmenos 1980). For the most basic configuration shown in Figure 10, this leakage degrades the performance of such a system by between 20 and 30dB compared to a well designed pulsed radar. Reflected power cancellers (Beasley and Stove 1991) can be implemented to reduce the leakage, which allow powers in excess of 250mW to be transmitted. However, at this time, the added complexity and expense do not make these practical for cost sensitive mining applications. These limitations notwithstanding, the following sections confirm that transmitted powers of only 10mW are sufficient for all of the applications discussed in this paper.

### **Making the Choice**

As all of the technologies described can achieve the required range resolution, the selection must be based on marginal performance differences, complexity and reliability.

#### **Narrow Pulse**

- Best understood technology
- Very short pulses difficult to achieve
- Needs transmitter and local oscillators
- High peak transmitter power required
- Blanking range problems (receiver recovery)

#### **Stepped Frequency**

- Requires stable phase locked source
- Good accuracy
- Complex signal processing
- Blanking range problems (pulse length)

## FMCW

- Conceptually simple
- Single millimetre wave oscillator
- Chirp linearity issues
- Sensitivity issues with reflected power

The FMCW option was selected as the most simple and, hence, the lowest cost and most robust of the three options.

### Hardware Selection

The first radar developed was the unit for measuring the depth of ore-passes. To perform the hardware selection, a number of manufacturers of millimetre wave components and systems were approached to quote on both the RF components that make up the front end and a complete system at either 77 or 94GHz.

Documentation on the performance of the potential systems was analysed to determine whether they would be suitable for the application as there was a concern that radars tailored for automotive detection requirements (typical target RCS of  $1\text{m}^2$ ) at 77GHz (Nagy and Wilhelm 1996) might not be sufficiently sensitive to detect low reflectivity rock targets, where the RCS could be smaller by a factor of twenty.

It is also understood that many of the radars produced for the automotive market are pulsed Doppler units which are not suitable for these applications. One exception was the closed loop linearised FMCW unit manufactured by Celsius Tech (now Saab Bofors), the performance of which was evaluated.

Front ends proposed by Quinstar, Millitech and Farran use Gunn voltage controlled oscillators (VCOs) and are based on the standard FMCW configuration shown in Figure 9. In each case, the tuning characteristics of the oscillators are rather non-linear as shown in Figure 11. To illustrate the differences in the bandwidth and linearity of VCOs supplied by these companies, the measured characteristics of each have been shifted so that the centre frequency,  $f_c$ , is the same. It can be seen from Figure 11 that sophisticated chirp linearization circuitry would be required to achieve a linearity of better than 1% for a sufficiently good range resolution.

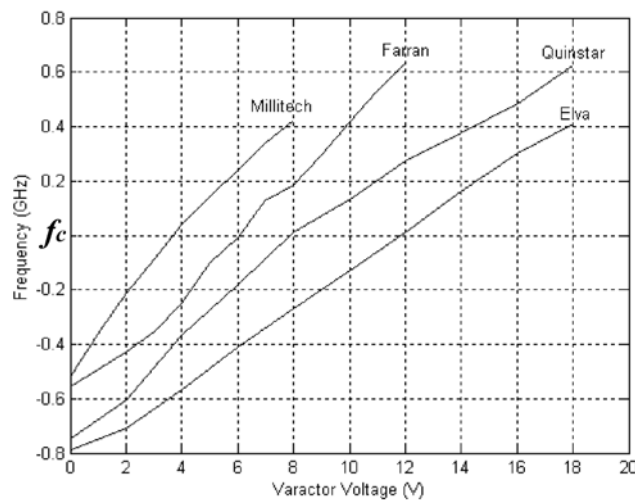


**Figure 5: Comparison between the relative millimetre wave VCO tuning characteristics from various suppliers**

The Elva unit operates with a low frequency VCO followed by an active IMPATT multiplier to produce an extremely linear tuning characteristic. This reduces the complexity of the external electronics, which compensates to some extent for the size and complexity of the unit itself.

An Elva unit was acquired and compared to the performance of units built up with other manufacturers' components and evaluated previously, and it was selected as the building-block sensor of choice for all of the applications because of its performance (due primarily to the good linearity), robustness and low cost.

The basic structure of the different radar systems discussed in this paper is shown schematically in Figure 12. All of the radars are based on the same FMCW ranging module and horn lens antenna. In each case, however, the total chirp bandwidth and duration are adjusted by controlling the output of the ramp generator, to suit the application. Additional hardware required by the sensors includes an anti-aliasing and signal conditioning module, and analog to digital converter board and a computer to perform the signal processing function. IO modules are also required to interface to the keyboard and display, and to communicate the radar information to the outside world.

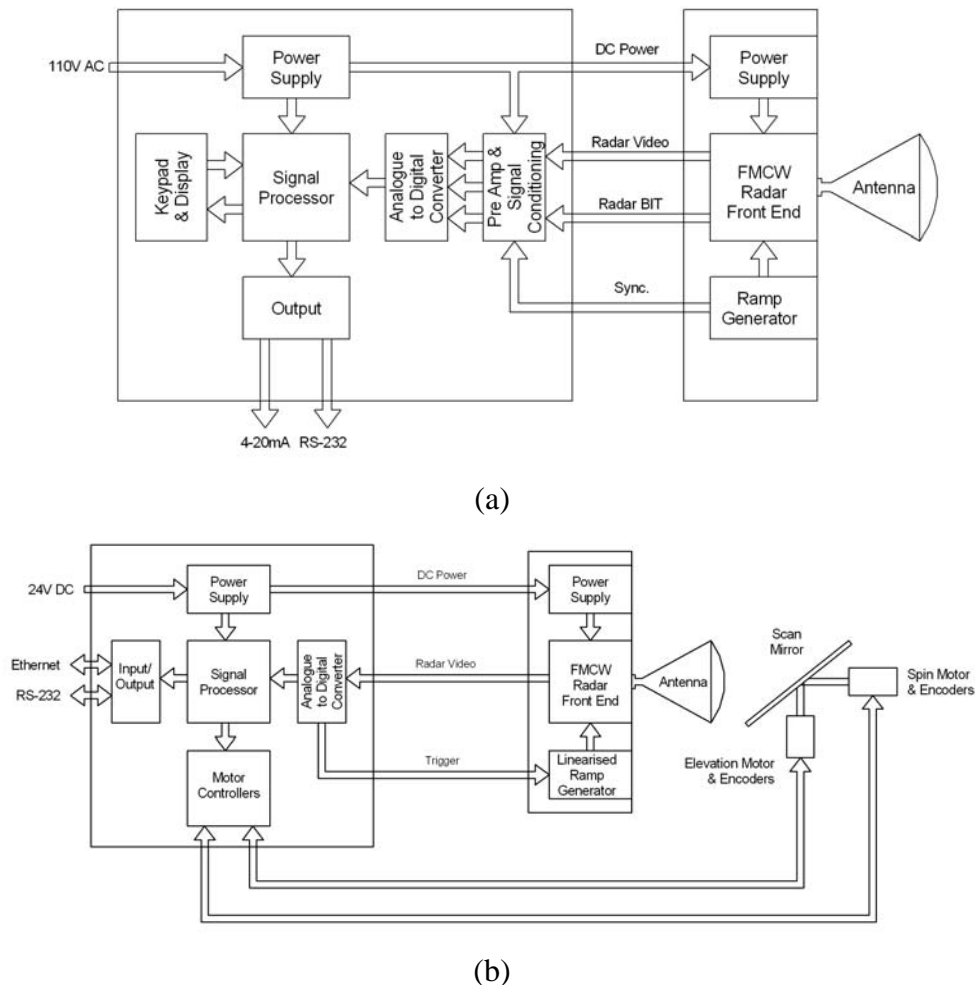


**Figure 12: Schematic diagrams showing similarities in the architecture of the radars with (a) being the ore-pass and bucket-fill and (b) the stope and dragline applications**

It is obvious from equation (13) that as the chirp bandwidth is increased the range resolution will improve, but simultaneously the total non-linearity increases and the range resolution

degrades. For a quadratic nonlinearity, the combined effect can be determined by

$$\delta R = \sqrt{\left(\frac{c}{2\Delta f}\right)^2 + (R.Lin)^2} \quad (18)$$

This Elva module relies on a particularly linear 7GHz VCO which is multiplied up to 94GHz to generate a swept bandwidth of up to 1.6GHz at 94GHz. The measured linearity is about 1.6% over the full swept band and because it is proportional to the bandwidth, will decrease as the bandwidth is decreased. Everything else being equal, this allows the range resolution to be optimised for a particular operational range as shown in Figure 13.

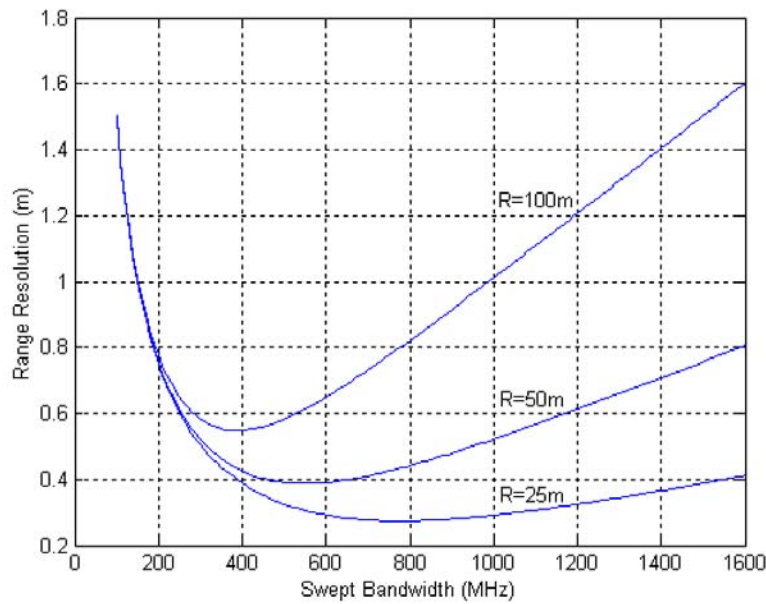


**Figure 13: Optimising the range resolution for a specific operational range**

The specifications of the four radar systems discussed in this paper are summarised in Table 3.

**Table 3: Radar Specifications**

	Ore-pass Radar (1D)	Bucket-fill Radar (2D)	Dragline Radar (3D)	Stope-fill Monitor (3D)
Transmit Power	10mW	10mW	10mW	10mW
Centre Frequency	94GHz	94GHz	94GHz	94GHz
Sweep Bandwidth	250MHz	1GHz	320MHz	530MHz
Sweep Linearity	<0.25%	<1%	<0.3%	<0.5%
Range Resolution	1.2m @ 100m	0.2m @ 10m	0.6m @ 100m	1.35m @ 250m
Maximum Range	120m	16m	100m	250m
Antenna Gain	42dB	42dB	42dB	42dB
3dB Beamwidth	1.5deg	1.5deg	1.5deg	1.5deg

#### IV. THEORETICAL RADAR PERFORMANCE

The radar performance is determined by the target echo signal to noise ratio (SNR) and signal to clutter ratio (SCR). In the presence of an attenuating medium, the SNR is determined using the radar range equation.

##### Received Echo Power

In regions of heavy dust or rainfall where atmospheric attenuation may be significant, the range equation (5) must be updated to include an attenuation term before the received echo power can be calculated.

$$S_{dB} = P_{dB} + 2G_{dB} + 10\log_{10}\left(\frac{\lambda^2}{(4\pi)^3} \cdot \frac{\pi\theta^2}{4}\right) - L_{dB} + \sigma_{dB}^o - 20\log_{10} R - 2\alpha R_{km}. \quad (19)$$

The probability of detecting this echo signal is determined by the SNR, and so to perform this function, it is also necessary to determine the received noise power.

##### Received Noise Power

The receiver noise power is a function of the effective temperature of the radar system which generates thermal noise and the bandwidth of the receiver.. To determine these parameters requires some knowledge of the operational principles of the FMCW radar.

The relationship between the frequency resolution,  $\delta f_b$  (Hz), and the range resolution,  $\delta R$  (m), of an FMCW radar can be determined (Brooker et al. 2005)

$$\delta f_b = \frac{2\Delta f \delta R}{T_b c}, \quad (20)$$

where  $\Delta f$  (Hz) is the swept bandwidth of the transmitter,  $\delta R$  (Hz), is the range resolution,  $T_b$  (s) is the sweep time and  $c$  (m/s) the speed of light.

To maximise the received SNR, the receiver bandwidth,  $\beta$  (Hz), which corresponds to the bandwidth of a single FFT bin, should match the frequency resolution of the radar. This in turn determines the thermal noise power, which contributes to the receiver noise level

$$N = 10\log_{10}(kT\beta) + NF \quad (21)$$

where  $k$  is Boltzmann's constant ( $1.38 \times 10^{-23}$  J/K),  $T$  is the system temperature (290K) and  $NF$  is the receiver noise factor. The latter is a function of the radar characteristics and varies from about 20dB for the ore-pass radar up to 30dB for the other radars because of the additional reflected power introduced by the scanning mirror and radome.

Table 4 shows the optimum receiver bandwidth (matched) and the system noise floor for the four different radar systems.

**Table 4: Radar receiver bandwidth and noise floor**

	Ore-pass Radar	Bucket-fill Radar	Dragline Radar	Stope-fill Monitor
Swept Bandwidth $\Delta f$	250MHz	1GHz	320MHz	530MHz
Sweep Time	1.1ms	220 $\mu$ s	440 $\mu$ s	1.76ms
Receiver Bandwidth $\beta$	1.95kHz	12.7kHz	6.34kHz	1.59kHz
Noise Floor $N$	-121dBm	-103dBm	-106dBm	-112dBm

As it is thermal in nature, the receiver noise can be assumed to be zero mean, white and Gaussian,

$$p(v) = \frac{1}{\sqrt{2\pi\psi_o}} \exp\left\{-\frac{v^2}{2\psi_o}\right\}, \quad (22)$$

where  $p(v)dv$  is the probability of finding the noise voltage,  $v$ , between  $v$  and  $v+dv$ . and  $\psi_o$  is the variance of the noise voltage.

If this Gaussian noise is passed through a narrow-band filter such as a single range bin output from the FFT used to process the FMCW radar spectrum, then the envelope of the noise voltage output will have a Rayleigh PDF (Skolnik 1980)

$$p(R) = \frac{R}{\psi_o} \exp\left\{-\frac{R^2}{2\psi_o}\right\}, \quad (23)$$

where  $R$  is the amplitude of the envelope of the filter output.

To determine whether a target is present in a specific range bin, the voltage signal level in that bin is monitored and if it exceeds a predetermined threshold,  $V_t$ , then it is assumed that a target echo is present. However, there is a finite, albeit small, possibility that noise alone may exceed the threshold in which case a false alarm has occurred.

#### Probabilities of False Alarm and Detection

The probability of a false alarm occurring,  $P_{fa}$ , is determined by integrating the tails of Rayleigh noise PDF from threshold voltage,  $V_t$ , out to infinity

$$\text{Prob}(V_t < R < \infty) = \int_{V_t}^{\infty} \frac{R}{\psi_o} \exp\left\{-\frac{R^2}{2\psi_o}\right\} dR = \exp\left\{-\frac{V_t^2}{2\psi_o}\right\} = P_{fa}. \quad (24)$$

For most radar applications the value of this integral is kept as low as possible while still maintaining a reasonable probability of detecting a target echo.

As shown earlier in this paper, the target echo from an FMCW radar consists of a sine wave, which in this case is assumed to have an amplitude  $A$ , and a frequency equal to the centre frequency of the FFT bin being examined. If this signal is present along with the noise at the input to the FFT, then the post FFT signal, after detection will have the following Ricean distribution (Skolnik 1990).

$$p_s(R) = \frac{R}{\psi_o} \exp\left\{-\frac{R^2 + A^2}{2\psi_o}\right\} I_0\left(\frac{RA}{\psi_o}\right), \quad (25)$$

where  $I_0(Z)$  is the modified Bessel function of order zero and argument  $Z$ .

The probability that the signal will be detected is the same as the probability that the envelope,  $R$ , will exceed the threshold  $V_t$

$$p_d = \int_{V_t}^{\infty} p_s(R) dR = \int_{V_t}^{\infty} \frac{R}{\psi_o} \exp\left\{-\frac{R^2 + A^2}{2\psi_o}\right\} I_0\left(\frac{RA}{\psi_o}\right) dR. \quad (26)$$

This cannot be evaluated in a closed form and so numerical techniques or series approximations have been derived. The following formula is in common use and is considered to be a good approximation.

$$P_d = \frac{1}{2} \operatorname{erfc} \left( \sqrt{-\ln P_{fa}} - \sqrt{\operatorname{SNR} + 0.5} \right). \quad (27)$$

Tables or graphs of the  $P_d$  as a function of the SNR with the  $P_{fa}$  as a parameter for non-fluctuating targets have been produced and one is reproduced from (Blake 1986) in Figure 14.

When detecting the presence of ore in a pass or building up a 3D surface from a large number of independent measurements, a reasonable detection probability would be 0.5 with a false alarm probability of  $10^{-4}$ . This equates to a signal to noise ratio,  $\operatorname{SNR} = 9.5\text{dB}$  as read directly from the graph.

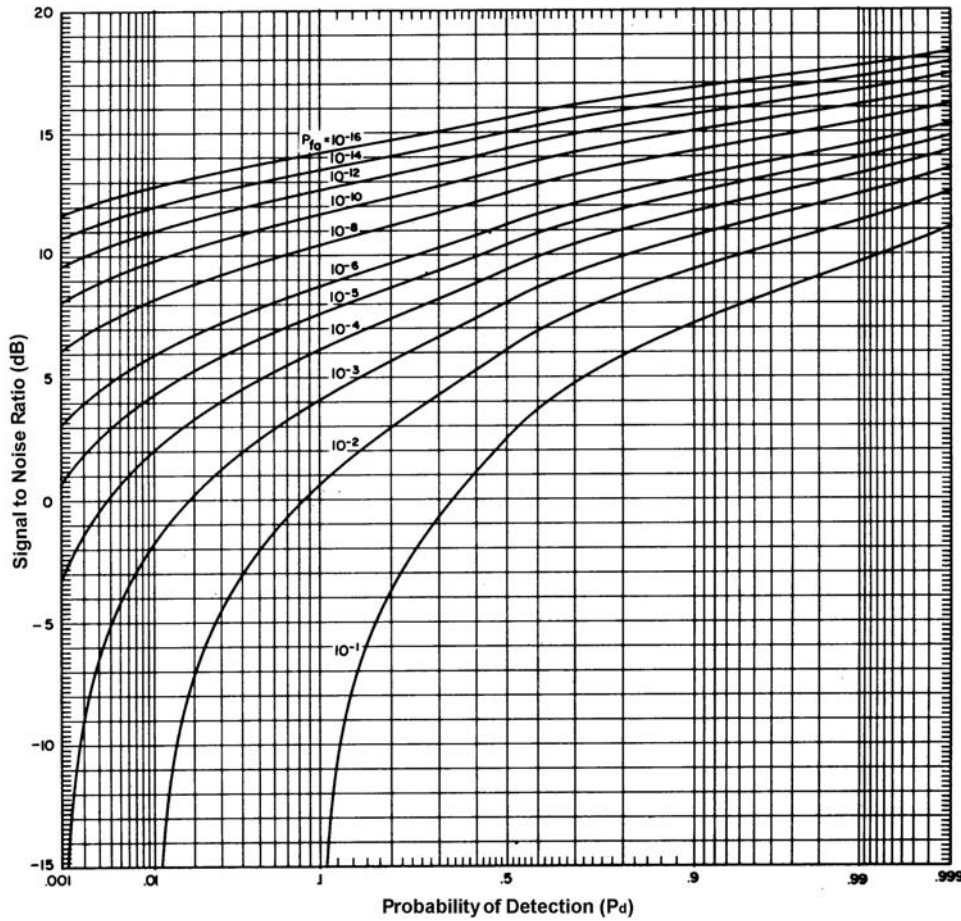


**Figure 14: Detection probability as a function of signal to noise ratio with false alarm probability as a parameter for a non-fluctuating target**

### Signal to Noise Ratio and Signal to Clutter Ratio

The signal to noise ratio can be determined graphically by plotting the received echo power and the noise floor on the same axes as shown in Figure 15. In this example, an extremely high attenuation environment of 12dB/km is assumed, which is equivalent to operation through fog with a visibility of 4m or rock dust with a visibility of less than 0.5m. In addition a fairly low mean rock reflectivity of -20dB is assumed. This graph can then be used to determine the maximum operating range for the radar given the specified  $P_d$  and  $P_{fa}$ .

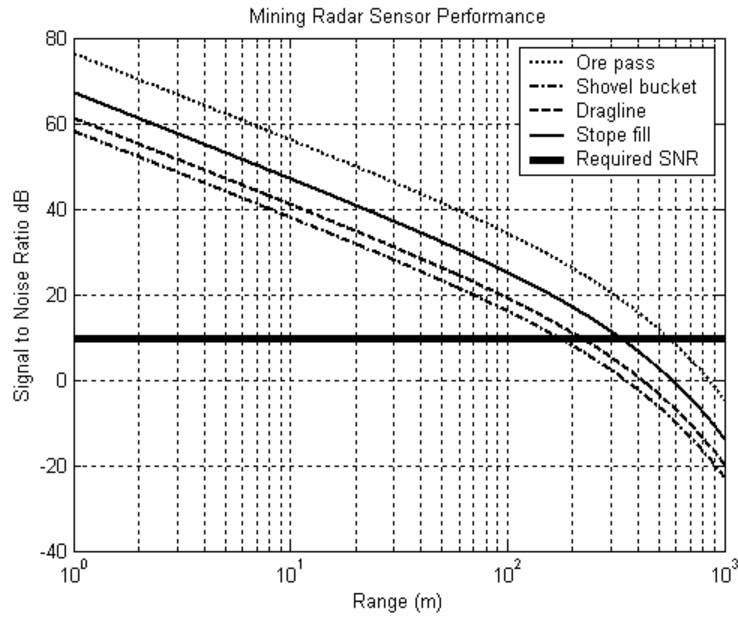


**Figure 15: Signal to noise ratios for reflection from the rock face of the four radar systems**

It can be seen from Figure 15 that the longest detection range is achieved by the ore pass radar with a range of about 550m, this is because both the receiver noise figure and the FFT bin size, which equates to the receiver bandwidth are low. In the cases of the scanned radars, the noise figure is higher by 10dB, and the bandwidth is increased to accommodate the faster update rate required. The stope fill monitor should be capable of detecting a rock face at a range of 350m as it can scan reasonably slowly. The detection range for the dragline radar is about 230m and that of the shovel bucket radar down at only 180m because it has the widest bandwidth. In each case, the theoretical range performance exceeds the required operational range by a significant margin. However, given the variability in the value for reflectivity, this safety margin is essential.

The signal to clutter ratio is the ratio of the signal power level to the clutter power level in the same range bin. The target RCS is the product of the reflectivity,  $\sigma^o$ , and the area of the beam footprint,  $A_{foot}$ , while the radar cross-section of the dust and water vapour within a single range bin is given by the product of the backscatter coefficient,  $\eta$ , and the volume of a resolution cell. This volume can be approximated by that of a cylinder with a cross sectional area  $A_{foot}$  and a length equal to the range resolution of the radar. Thus the SCR reduces to

$$SCR_{dB} = \sigma_{dB}^o - 10\log_{10}(\delta R \eta). \quad (28)$$

For a visibility of 10m, the backscatter coefficient of water vapour and coal dust are respectively  $-90\text{dBm}^2/\text{m}^3$  and  $-97\text{dBm}^2/\text{m}^3$  (Brooker 2008). Using this value results in the signal to clutter ratios listed in Table 5.

**Table 5: Radar signal to clutter ratio for water vapour and for coal dust**

	Ore-pass Radar	Bucket-fill Radar	Dragline Radar	Stope-fill Monitor
Water vapour (vis. 10m)	69dB	77dB	72dB	69dB
Coal dust (vis. 10m)	76dB	84dB	79dB	76dB

From this table, it is clear that the backscatter returns from even the most dense fog or dust have an almost insignificant effect on the performance of radars in mining environments, and so can be ignored.

## V. IMPLEMENTATION

To facilitate their installation, mounting and alignment, the sensors were each built as two modules comprising a front end and a separate signal processor connected by a shielded umbilical cable. It can be seen in Figure 16 that all of the sensors use the same robust 150mm diameter housing as the ore-pass unit. In each case a mirror scanner has been appended to the antenna flange so that the beam can be directed.

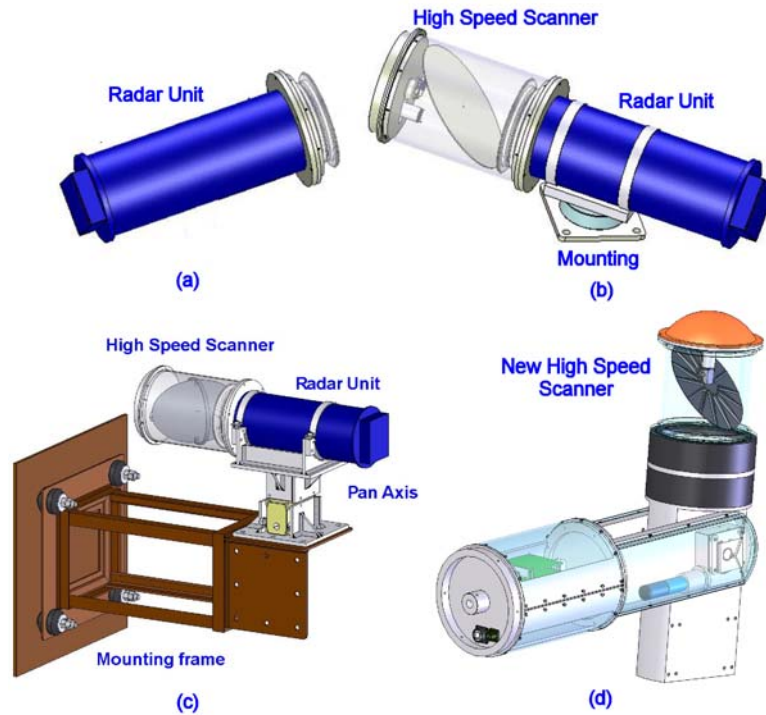


**Figure 16: Evolution of the sensors from a common module from (a) Range only radar (b) 2D radar for profiling (c) 3D radar for outdoor imaging and (d) 3D radar for insertion through a bore-hole**

In the Ore-pass radar design, the alignment flange was incorporated into the end-plate to simplify the design. The signal processor, power supplies and displays were built into a commercially available housing with power and signal access via cable glands and a mil-circular connector.

To allow for installation by a single technician, the masses of the two modules were both kept as low as possible, with the processor box weighing in at 4.7kg and the front end (without mirror scanner) at 5.1kg.

### Scanner Design

The bucket-fill radar required a high speed mirror scanner to produce 2D scans across the bucket as shown in Figure 1d. This was implemented using a standard swash-plate design shown in Figure 16b. With careful balancing, this configuration is capable of scanning a  $1.5^\circ$  beam at up to 20rps. The top speed of the mirror is governed not only by the dynamics of the structure but also by the mirror motion, which induces the Doppler shift and consequently spreads the echo spectrum and reduces the range resolution.

For the mirror moving at 20rps, the speed at the periphery of a 0.15m diameter mirror is

$$v = 20\pi D = 9.4\text{m/s} . \quad (38)$$

This results in a Doppler shift of

$$f_d = \frac{2v}{\lambda} = 5.9\text{kHz} . \quad (39)$$

As half of the mirror is travelling towards the target, and the other half away, the received signal will be spread by a maximum of double this amount (11.8kHz). This is a little smaller than the receiver bandwidth of this radar. The distribution of this frequency spread is determined by weighting the linear distribution of the Doppler shift across the mirror by the mirror area and the taper on the illuminating antenna beam. In essence, the Doppler shift generated by a mirror rotating at 20rps spreads the return from a point target to the extent that the signal power appears in multiple bins and so degrades the range resolution and reduces the detection probability by decreasing the signal to noise ratio.

One of the innovations of the scanner is that the scan speed can be adapted to optimise performance for specific applications. For example, in the shovel-bucket application the mirror should be scanned at the appropriate speed to maximise the number of hits on the target surface. This will in turn depend on the speed at which the bucket is being drawn through the beam.

### **Mirror Design**

Two types of mirrors have been designed, the first is completely flat and generates a pencil-beam. This is used for 2D profile generation using the beamwidth-limited imaging modality. The second mirror design is slightly curved and generates a fan-beam with the narrow beam aligned to the axis of rotation. This produces 2D reflectivity images using the range-gate limited imaging modality.

### **Signal Processing**

The beat signal output by the radar is first filtered by an anti-aliasing filter after which it is sampled and digitised at the appropriate rate. A block of data corresponding to samples taken over a single sweep period,  $T_d$ , is shaped by a Hamming window to reduce range sidelobe levels before the range spectrum is obtained by processing through an FFT. Multiple sweeps can be integrated to improve the available signal to noise ratio prior to the application of the target detection, peak interpolation and discrimination algorithms.

### **Integration**

Signal integration is accomplished by averaging the magnitude of the post FFT range spectra. This is known as post-detection or non-coherent integration and is less effective than performing the function on the complex signal. It is, however, more practical in these applications as coherent integration requires that signal phase coherence is maintained from sweep to sweep, and that is not always possible from a moving, or even vibrating, platform.

For non-coherent integration (Skolnik 1980), the effective number of sweeps integrated can be approximated by

$$N_{eff} \approx N^{0.8} , \quad (40)$$

where  $N$  is the actual number of sweeps integrated, and is determined by the time available between measurements and the rate at which the beam is being scanned. In the ore-pass case, where the update rate can be slow, sixteen measurements are usually averaged to produce an

improvement in SNR of  $8 \cdot \log_{10}(16) = 9.6\text{dB}$ . In the scanned dragline and stope applications, the number of measurements integrated is usually smaller (typically between 1 and 4), while in the bucket-fill application, the signal is generally not integrated as the processing throughput is governed by the time it takes to execute the FFT algorithm.

**Peak Detection**

Once a spectrum has been obtained, it is necessary to identify the returns from the targets of interest. This is achieved using a constant false alarm rate (CFAR) process as illustrated schematically in Figure 17.

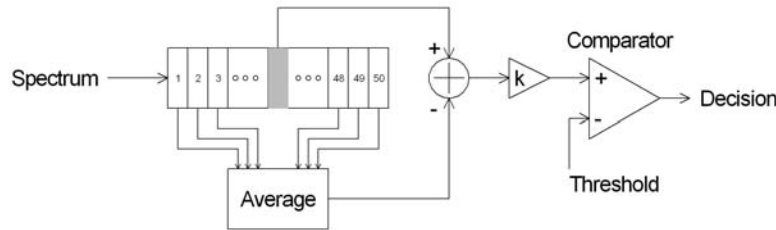


**Figure 17: Multiple cell averaging CFAR**

Needless to say, target detection using the CFAR process introduces additional losses as the statistics are incompletely characterised. For example, a cell averaging process will exhibit a 0.6dB loss for a 50 cell estimator (Skolnik 1980). In Figure 18, where a 25+25 point moving average is used to determine the value of the signal, it can be seen that the CFAR process detects the two targets without detecting the noise, whereas a constant threshold would also detect the noise floor at short range.

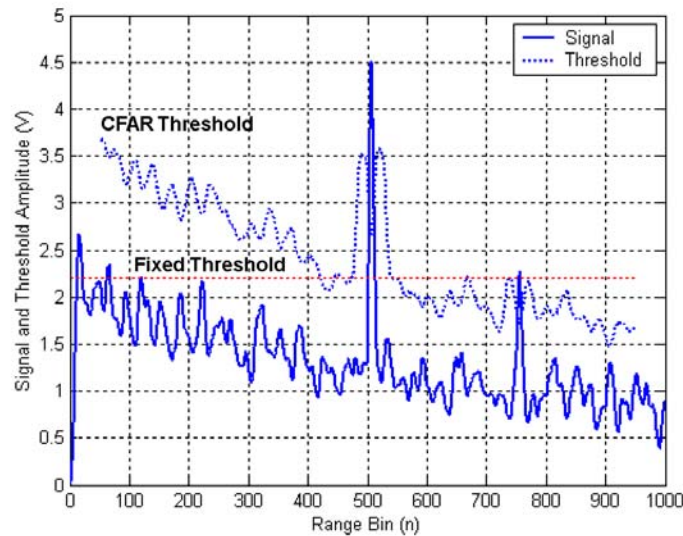


**Figure 18: CFAR performance for a sloping noise floor as a comparison with a fixed threshold**

Ground returns often include a number of peaks which exceed the CFAR threshold, therefore a second process identifies these peaks by searching for range bins whose amplitude is greater than those on either side of it. Finally, these peaks can be further processed by selecting all, all within a window, the largest, or the peak at the longest range as required by the application.

### Range Interpolation

Using a finite length FFT to process the FMCW signal results in a range measurement quantised into bins, with the bin containing the largest amplitude peak corresponding to the range to the target. However, due to various effects, the signal is not constrained to only one bin but appears in adjacent bins with reduced amplitude.

If the amplitudes of the signals on each side of the peak are equal, then it can be concluded that the true range corresponds to the range at the centre of the bin. However, if the arrangement of amplitudes is asymmetrical, then the peak lies somewhere between the bins with the highest amplitudes. Quadratic interpolation is used to improve both the estimate of frequency and the estimate of the signal level of the output of an FFT.

Figure 19 shows the measured and interpolated amplitude and range error as the true target range moves from bin 120 to 130.

Without interpolation, the normalised range error can vary by up to one half bin (+/-0.5), while with interpolation, the variation is less than 0.01. This corresponds to a measurement accuracy of about 10mm for the ore-pass radar case and even less in the other, higher range resolution, applications.

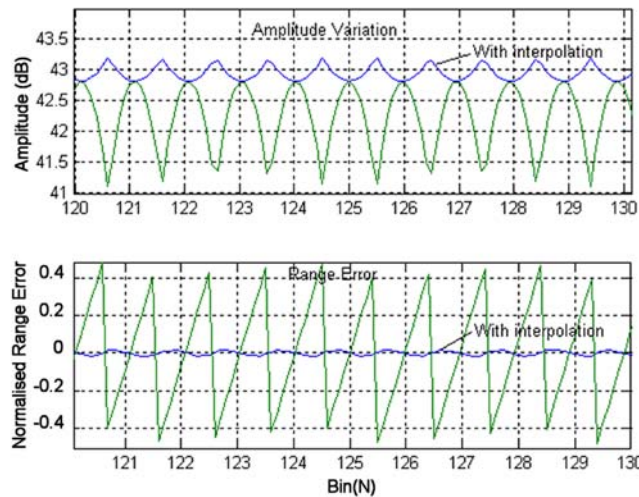


**Figure 19: Quadratic interpolation showing improvements in the measured signal amplitude and the measured range that can be achieved for a “point” target return using this technique**

For a quadratic defined by the equation  $y = ax^2 + bx + c$ , the peak lies at an offset from the central bin of  $\Delta x = -b/2a$ . If the peaks of the three bins are defined by points  $(-x, y_1), (0, y_2), (x, y_3)$ , it is possible to solve for  $a, b, c, \Delta x$  and for the amplitude of the peak  $\hat{y}$

$$\begin{aligned} a &= (y_1 + y_3 - 2y_2) / 2x^2 \\ b &= (y_3 - y_1) / 2x \\ c &= y_2 \end{aligned} \quad (41)$$

$$\Delta x = \frac{-b}{2a} = \frac{x(y_1 - y_3)}{2(y_1 + y_3 - 2y_2)} \quad (42)$$

$$\hat{y} = a\Delta x^2 + b\Delta x + c \quad (43)$$























